

Visualization and analysis of LiDAR waveform data

Richard C. Olsen, Jeremy P. Metcalf,

Remote Sensing Center, Naval Postgraduate School, Monterey, CA 93943

ABSTRACT

LiDAR waveform analysis is a relatively new activity in the area of laser scanning. The work described here is an exploration of a different approach to visualization and analysis, following the structure that has evolved for the analysis of imaging spectroscopy data (hyperspectral imaging). The waveform data are transformed into 3-dimensional data structures that provide xy position information, and a z-coordinate, which is the digitized waveform. This allows for representation of the data in spatial and waveform space, the extraction of characteristic spectra, and the development of regions of interest. This representation allows for the application of standard spectral classification tools such as the maximum likelihood classifier.

Keywords: LiDAR, terrain classification, waveform LiDAR, Optech Titan

1. INTRODUCTION

Light detection and ranging (LiDAR) systems have evolved rapidly over the last decade. Consistent commercial operations have been conducted over that time, and research activities, primarily exploiting the timed returns termed a “point-cloud”. Extensive applications and tools exist for such data. Relatively less common use has been made of digitized waveforms. Waveform data has been slow to emerge, data formats are awkward, and the tools limited. There is a rather specialized body of work on waveform analysis in bathymetric applications¹, work on large-footprint terrestrial and satellite systems^{2,3}, and then a modest amount of work on small-footprint terrestrial systems beginning roughly in 2003^{4,5,6}.

Analysis techniques applied to small-footprint airborne scanner data have generally focused on the problem of more robust extraction of ground returns⁷, or have extended into fitting Gaussian distributions to the digitized returns.^{8, 9, 10, 11, 12} A modified approach is to use moments of the spectra, or moments of the distribution function for returned energy.¹³ The above techniques generally make some compensation for range effects, but do not deal with complexities caused by illumination angle. One innovative approach is to “voxelize” the data, producing pseudo-waveforms corresponding to vertical profiles that are more directly inter-comparable.^{14, 15}

One consistent factor with the previous work is that there appears to have been relatively little work in directly viewing the full datasets, or directly using the spectra. The work described here is an initial look at processing the full LiDAR waveforms for display, and the application of analysis techniques derived from spectral imaging.

2. OBSERVATIONS

Data were collected over the Monterey Peninsula on June 5, 2016. Teledyne Optech’s Titan Multispectral LiDAR system uses three independently-scanning lasers to collect data at a combined ground-sampling rate of 1 MHz. Titan’s three laser channels are as listed: Channel 1 operates in the SWIR at 1550 nanometers (nm). Channel 2 operates at 1064 nm, and channel 3 operates in the visible green at 532 nm. The system records all intensities in a 12-bit dynamic range. The 532 nm channel has a beam divergence of ~0.7 mrad; the other two sensors operated at ~0.35 mrad. The other noteworthy difference between the 3 channels is in pointing: channel 2 is nadir pointing, channel 1 is pointed 3.5 degrees forward; channel 3 is pointed 7 degrees forward. Waveform data were collected in Channels 2 & 3.

The data were delivered by the National Center for Airborne Laser Mapping (NCALM) in the native Optech waveform data format, and in PulseWaves format. This latter format was developed by Martin Isenburg to be somewhat sensor agnostic, allowing software to be applied to data from multiple platforms (e.g. Riegl, Optech, and Nikon)¹⁶.

*olsen@nps.edu; phone 1 831 656-2019; fax 1 831 656-2834; www.nps.edu/rsc

An alternative would be the newer 'las' formats, las 1.3 or las 1.4. Beyond the issues with the range of data formats, there were issues with processing platform (Windows™, MacOS™, Unix), and matching software (C, C++, MATLAB™, etc). Existing software for addressing the data seemed to either not work on any of our possible combinations, or simply did not provide the necessary functionality. As a result, software was created in Interactive Data Language (IDL), which then allowed for a transition to the Environment for Visualizing Information (ENVI).¹⁷ The current stage of analysis makes use of the data received in the PulseWaves format.

2.1 Collection Overview

The data are illustrated first in Figure 1, an elevation representation of the point cloud, with height scaled as color from 5 to 33 m. The area presented is the grounds of the Naval Postgraduate school. Data are from 79503-79524 s. Data are selected from channels 2 and 3, providing higher point density than either individual channel (the objective of the pointing design for the Titan sensor). The parking lots are largely empty because the collection occurred on a Sunday. This allows for a rather serendipitous opportunity to view largely unobstructed flat asphalt surfaces.

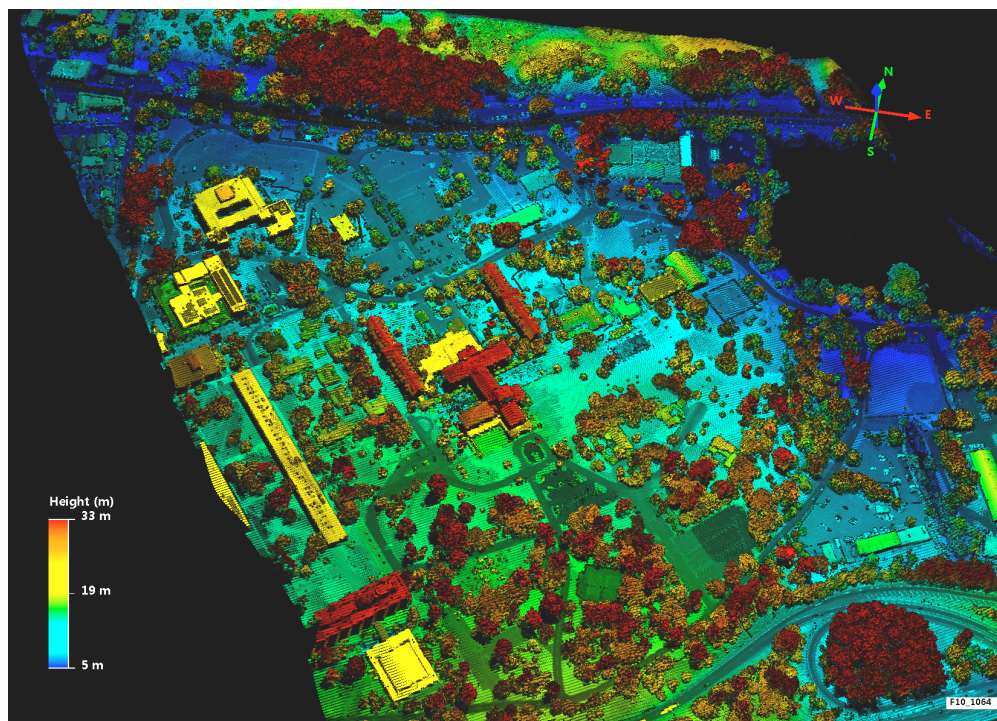


Figure 1. Point cloud data over the NPS campus, presented with height colored from blue to red (traditional rainbow color scale). The dark region to the upper right is the Del Monte Lake (only a meter or so deep, but murky). The scan line edge on the left reflects the aircraft flightline. The buildings along the flightline on the left are King Hall (yellow rectangle, at the bottom), a portion of Spanagel Hall (just above in red), and the long linear feature of Root Hall (yellow). Hermann Hall is mostly in red in the center of the frame.

The subtle differences in the two channels are illustrated in Figure 2, which shows a chip from flight-line 10 for the 532 nm (plotted in green) and the 1064 nm channel (plotted in red). Consequences of spectral variations in the point cloud are addressed in a companion paper.

The analysis process for the waveform data involved writing code in IDL to parse and input the PulseWaves formatted data, in order to enable analysis in IDL and ENVI. A significant amount of work went into sifting through the data structure and artifacts, including clouds. As part of this, a 'waterfall' display technique was evolved to view the data. One illustration is given here in Figure 3, which shows one mirror-scan of data.



Figure 2. Point cloud data over the NPS campus, perspective view, 532 nm (green), and 1064 nm (red). Display is focused on Herman Hall at the center of campus. The lower right portion of the figure is grass and trees. Color shading reflects intensity, scan pattern apparent for both sensors. Some differences will be due to the difference in pointing angles of the two sensors – the 1064 nm sensor is nadir pointing.

The top panel in Figure 3 is the intensity plotted in grey-scale for a few milliseconds of time (horizontal axis), and then sampled at ~ 1 GHz (vertical axis). The number of samples varied from shot to shot. For purposes of display and storage into a regular data structure, up to sixty waveform samples were selected, which appeared to be sufficient to capture most of the returns. Shorter returns were padded with zeroes up to 60. Figure 3 shows these samples – effectively the first return data. (As described briefly below, additional returns for each outgoing pulse were rare, and ignored for now.) The narrow horizontal band from 10-20 samples is the bulk of the return signal. The lower plot is the angle from nadir for the channel 2 sensor. The quantity plotted is based on the angle between the horizontal and vertical coordinate system, and is going to be similar to the pointing direction for the ± 30 degree mirror sweep. Unfortunately, the mirror angle is not included in the PulseWaves formatted data, so only this rather indirect value is available. The brightest returns clearly follow from the most nadir pointing.

The sensor output includes an average intensity for each shot, which is helpful in reviewing the data. The data format provides an average return intensity, scaled from 0-255. This parameter, and subsequently the full returns, was gridded using the xy position information taken from the “target” position as recorded in the PulseWaves format. Figure 4 shows the gridded data rotated such that the flight line is roughly vertical for convenience.

Figures 5 and 6 show the same sort of displays for the 532 nm sensor. The waterfall display is quite different, in two ways. The return pulse data are strongly peaked in the near-nadir direction (keeping in mind that the sensor is mounted with a 7° offset). The two illustrations (Figures 3 & 5) have not been adjusted to coincide with the same ground point, but rather have been arbitrarily selected at similar GPS time.

Figures 4 & 6 show rather dramatic differences in grey value distributions, representing the impact of different ground reflectance as a function of laser wavelength. Buildings show a much higher intensity contrast with the background at 532 nm.

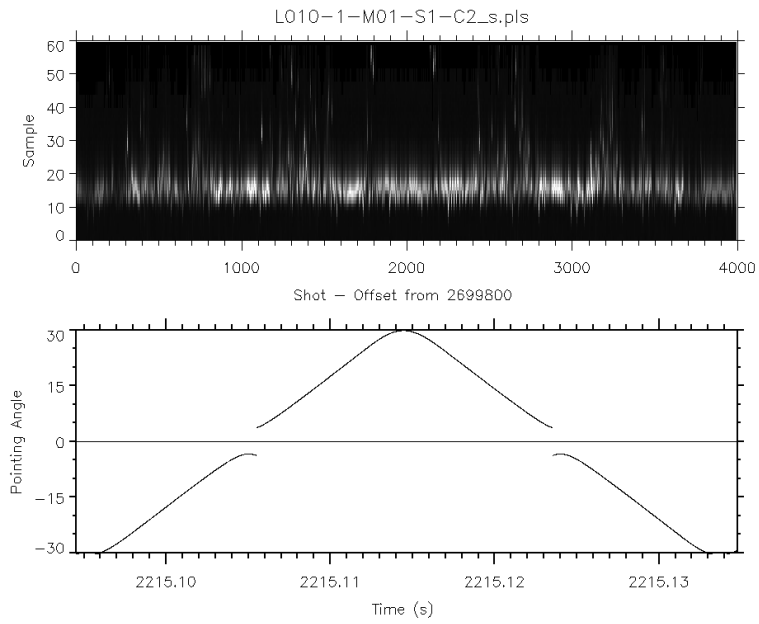


Figure 3. Waveform data, NPS campus, 1064 nm, scaled waterfall display (upper panel), for one mirror sweep. The lower panel shows the pointing angle.



Figure 4. Waveform data, NPS campus, 1064 nm, average intensity. Aside from the dark region of Lake Del Monte at top right, most of the other dark regions are roads and the campus parking lots.

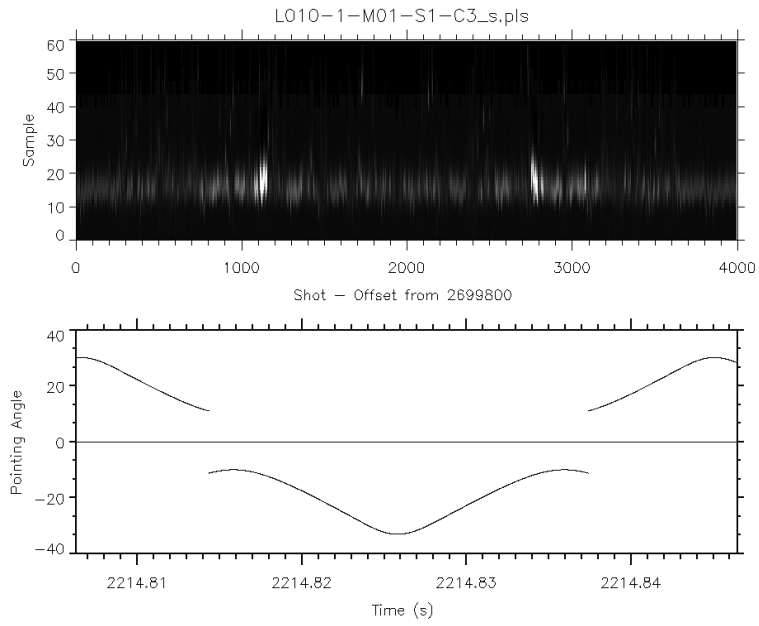


Figure 5. Waveform data, NPS campus, 532 nm, scaled waterfall display (upper panel), for one mirror sweep. The lower panel shows the pointing angle.



Figure 6. Waveform data, NPS campus, 532 nm, average intensity. There is a small grove of fairly dense trees (Eucalyptus) in the lower portion of the scene, encircled by the freeway 'cloverleaf', appearing to be quite dark in this scene.

A more subtle display is possible by viewing the data at a particular waveform bin – a differential slice in the ensemble of return data. Figures 7 & 8 show the data taken for what effectively is range-gate 18. The embedded histograms give a feeling for how the data values are distributed, and in particular the wider dynamic range found at 1064 nm than 532 nm in this instance.

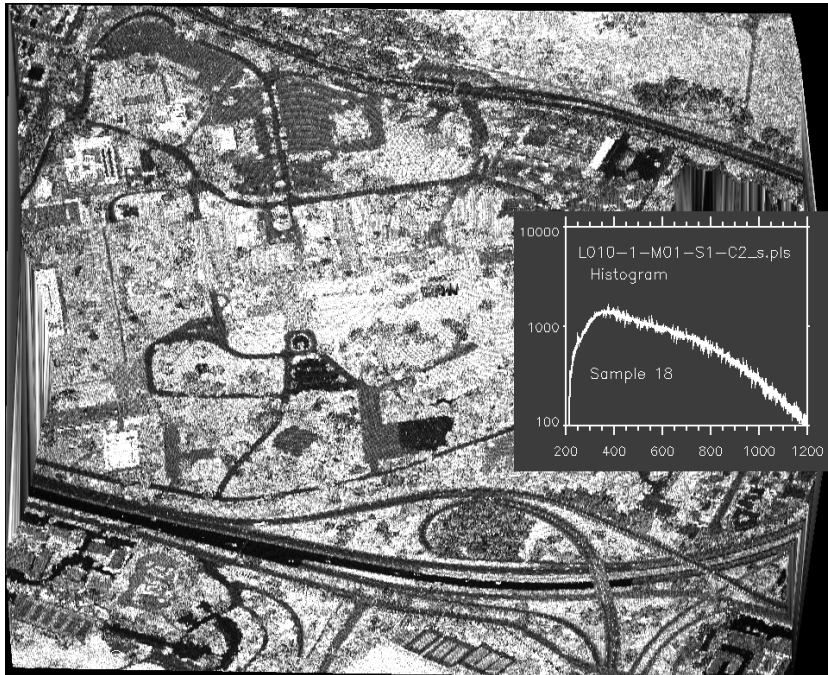


Figure 7. Waveform data, NPS campus, 1064 nm, intensity at waveform sample 18. The large areas of grass and other vegetation are bright at this wavelength.

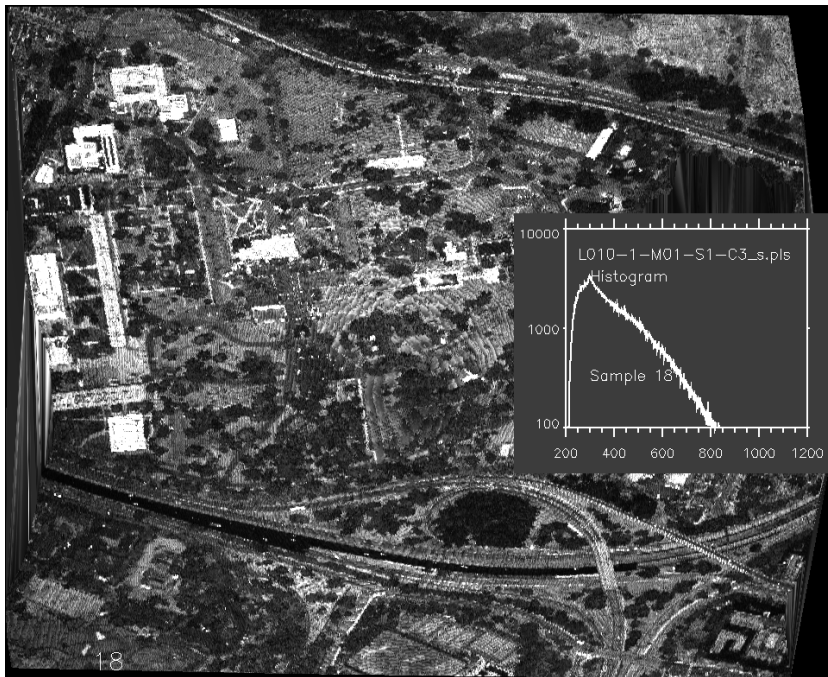


Figure 8. Waveform data, NPS campus, 532 nm, intensity at waveform sample 18. Buildings on the left side of the view again show much higher contrast to the ground level at this wavelength, though Hermann Hall with a red tile roof blends into the background in the center of the image (ref Figure 1).

With the data extracted from the PulseWaves format, it was possible to view the gridded waveform information in ENVI, as though it were a hyperspectral data set. To emphasize this rather fundamental point, a rather old tool from the world of spectral analysis is used, the hypercube. Figure 9 shows such an illustration. The xy coordinates in the display are primarily spatial location, with a projection along the sides in the spectral (waveform) direction. The top layer is an RGB triple (bands 15/20/25) for the 1032 nm sensor. The sides, in a rainbow color scale, show variations associated with reflectance at the boundaries of the 'cube'.

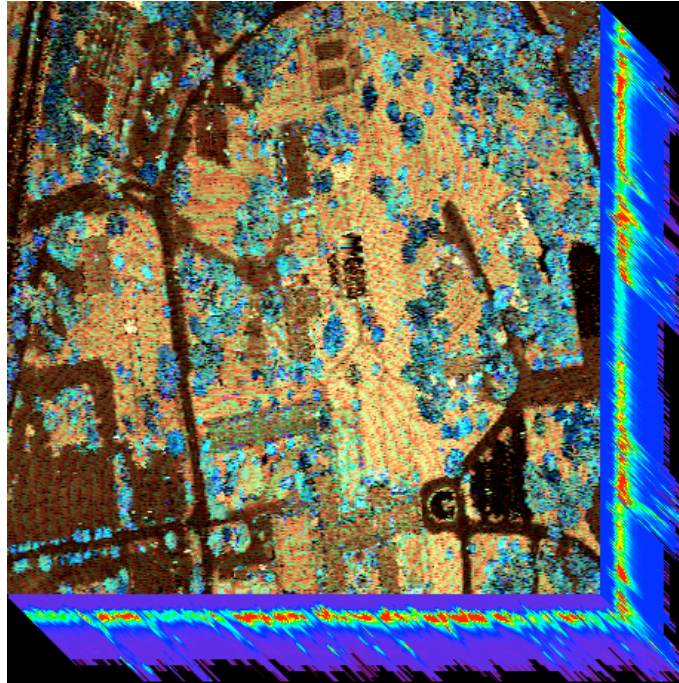


Figure 9. Waveform data, NPS campus, 1064 nm, hypercube display, waveform samples 15/20/25 in R/G/B channels. The blue or cyan areas are mostly trees, dark regions are asphalt (roads, parking lots), the yellow/orange regions are grass, or the tops of buildings. Spectra for edge elements of the hypercube are illustrated with a rainbow color scale.

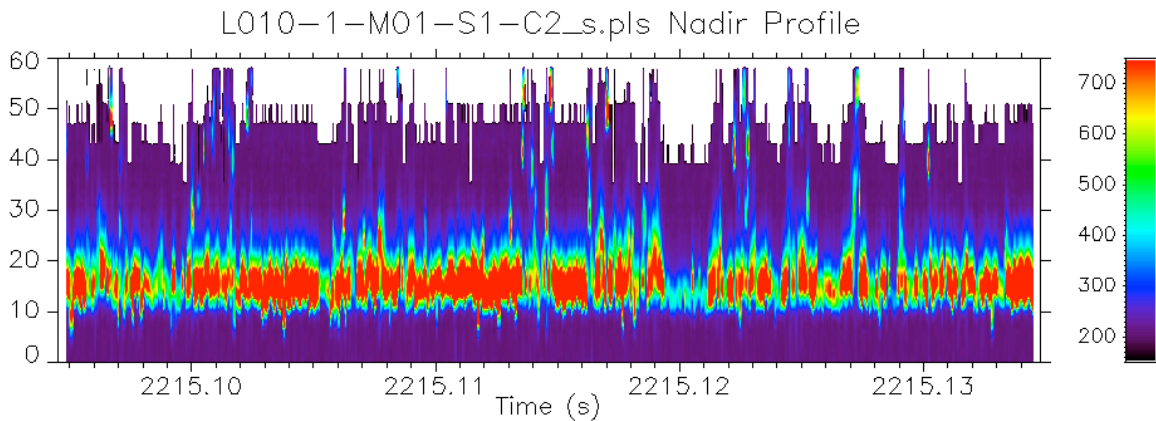


Figure 10. Waveform data, NPS campus, 1064 nm, along the nadir track (the vertical in Figures 6-9) These samples show the variation along the flight line. The dip at 2215.12s is associated with a parking lot. This figure corresponds to the rainbow scaled image segments on the edges of Figure 9. Truncation in the waveform returns is apparent in bins 50-60.

With the data now available in a standard analysis tool, it is possible to view, extract waveform spectra, and address tasks like waveform classification using the standard spectral toolkit. Figure 11 shows the 532 nm data in a three-color display, with bands assigned to RGB in an attempt to allow discrimination of different scene elements. Two illustrative spectra are extracted. There is a tennis court at the bottom of the scene, representing a flat surface, and a vegetated area near the center of the scene (a tree). Spectra for those two elements are shown in Figure 12. The vertical lines in Figure 12 indicate the three spectral bands chosen to build Figure 11. Figure 13 shows three representative spectra from channel 2 (1064 nm). The admittedly very Gaussian looking spectra are obvious motivation for curve fitting approaches to such data.

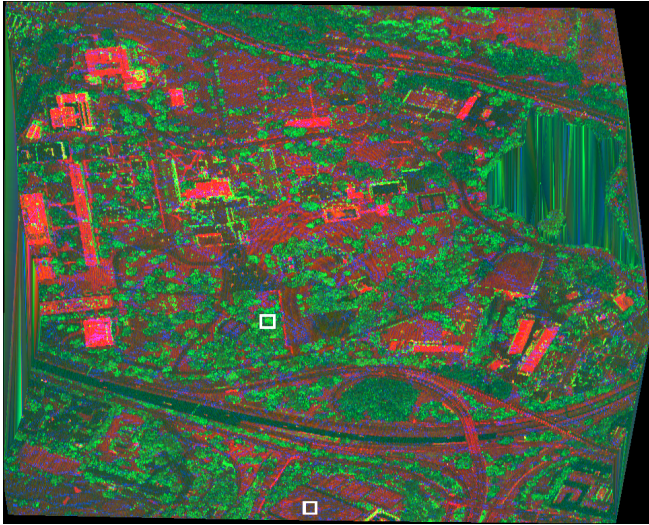


Figure 11. Waveform data, NPS campus, 532 nm, samples at r:18, G:29, B:10. The two white boxes indicate the two locations for which spectra were selected.

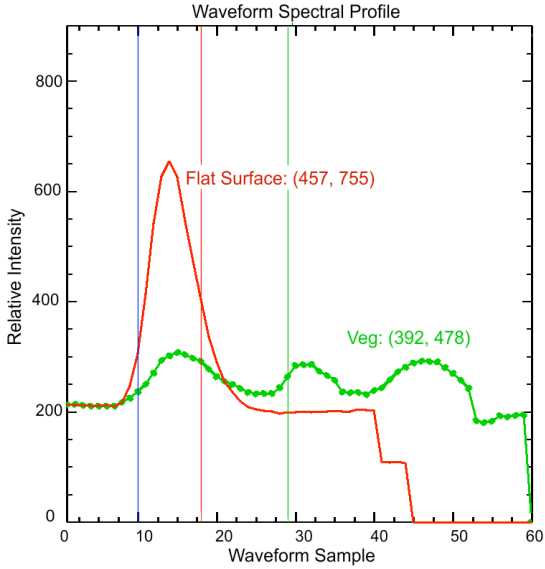


Figure 12. NPS campus, 532 nm, samples at R:18, G:29, B:10 indicated by vertical lines; spectra from a flat surface (not a building), and vegetation. Scene coordinates are relative to the image origin.

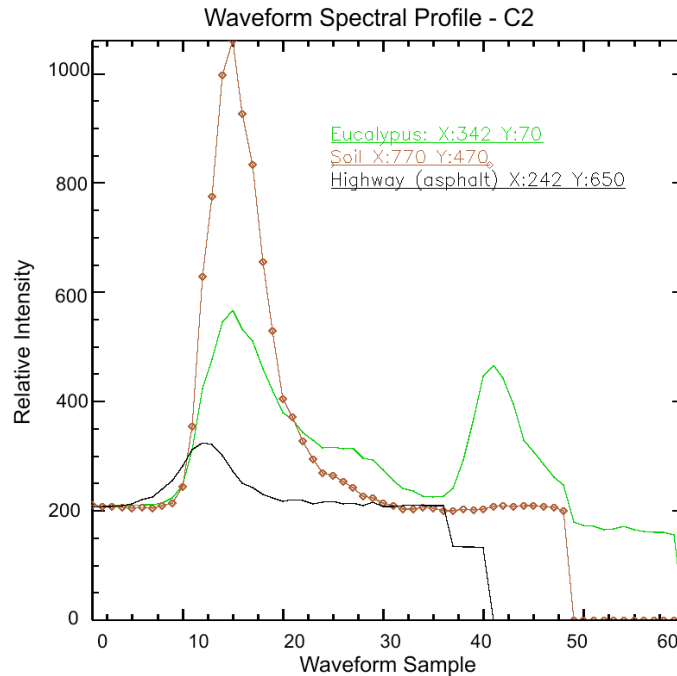


Figure 13. Characteristic spectra at 1064 nm are shown for three scene elements. There is a Eucalyptus grove at the top edge of the scene, used here for a tree spectrum, the soil is from the baseball field, and the asphalt spectrum is from the highway at the bottom of the scene. Scene coordinates are relative to the image origin. The sharp drop at waveform sample 49 in the soil spectrum is in some sense reflected for spectra plotted in Figure 10 – the digitizer terminated at that point.

Extending the concepts of use in spectral imaging, regions of interest were defined in the 1064 nm data, as illustrated in Figures 14 and 15. Figure 14 shows the 1064 nm data again, with the same color scheme used above in Figure 9 – bands 15/20/25 assigned to R/G/B. Figure 15a shows the representation found in the n-dimensional (n-D) visualizer in ENVI, with some of the characteristic clustering found in well-differentiated scene elements in spectral imagery. Figure 15b shows the spectra for a few representative regions. This interactive approach to analysis can be valuable in training classification techniques.

Several display techniques remain to be explored. The most obvious is to make use of the principal component (PC) transform, a standard technique for dimensionality reduction.¹⁸ The n-D visualizer can then be applied in the reduced dimensionality space of the PC transform. With some care, additional elements of the data, such as the value for Above Ground Level (AGL) can be added into the data representation as a variable.

The next step to be completed is a scene classification based on the waveforms. This has not been completed at this point, and remains for future work.

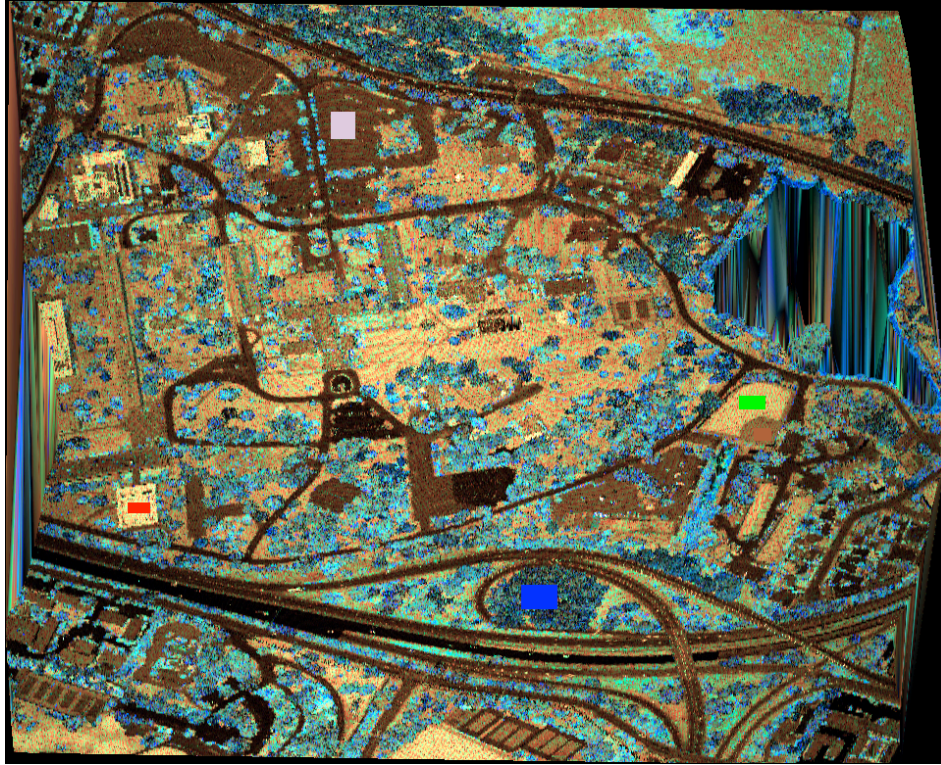


Figure 14. RGB representation of data taken at 1064 nm. Waveform samples 15, 20, and 25 were used

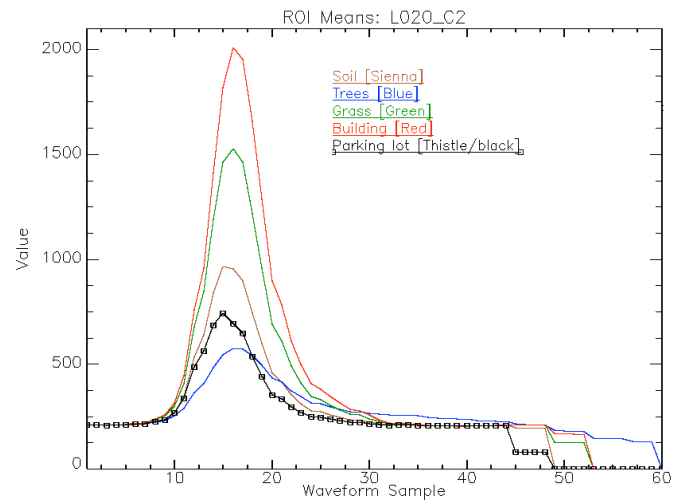
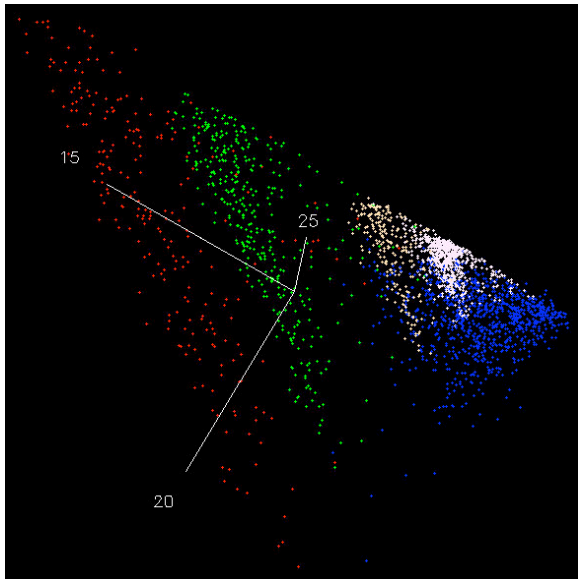


Figure 15. a) n-dimensional visualizer, bands 15/20/25, arbitrary projection; b) mean spectra from regions of interest (the asphalt data are plotted as 'thistle' in Figures 14 and 15a, as black here in 15b).

3. SUMMARY AND CONCLUSIONS

An approach to the visualization and analysis of waveform data has been illustrated here. Exploration of the data has proven viable, particularly once the data are available in a standard analysis tool. Analysis of the waveform data has not extended beyond this initial exploration of the data. Obvious next steps are to consider normalizing or calibrating intensity for range, to link the waveform data to the discrete point cloud, and linking the waveforms taken at two different wavelengths. It is not clear, yet, what the impact of differing view angles produces, including the angular offset between the scanners. Combining data from different flight-lines is problematic for the same reason. These are the issues addressed by the University of Texas group with their voxelized approach to waveform analysis^{13, 14}.

Classification of the data will also need to take advantage of the more usual LiDAR characteristics, including classification as ground, or not, and parameters such as the above ground level (AGL) variable. Challenges for this are to maintain consistent scalar variables, that is, data with dynamic ranges that are compatible for use in classification approaches like a maximum likelihood classifier. It would be useful to include classification from the point cloud (e.g. ground, tree, building), but this will require some adjustments because of the discrete nature of the classes.

Not apparent in any of the results presented here are the issues with returns following the first digitized return. There were not a great number in this data set, but in other data sets it has been seen that for each outgoing pulse, there are multiple return pulses captured and digitized. The scheme shown here will need to be modified to deal with such. The outgoing pulses are also detected and digitized. They have not been presented here, but there are variations in those pulses. There appears to be some jitter in the digitizer timing which is apparent in the outgoing pulse data that will need to be taken into account. Variations in the intensity of the outgoing pulses may also need to be considered.

The intended philosophical approach to the data was to maintain the full range of point returns. Presentation of the data has required rasterization of the waveform data, and some averaging/sampling issues are apparent. Subsequent work will focus on maintaining the full details of the spectra.

REFERENCES

- [1] Eren, F., Pe'eri, S., and Rzhanov, Y; "Airborne Lidar Bathymetry (ALB) waveform analysis for bottom return characteristics," Proc. SPIE 9827, Ocean Sensing and Monitoring VIII, 98270H (2016)
- [2] Wagner, W., Ullrich, A., Briese, C., "Der Laserstrahl und seine Interaktion mit der Erdoberfläche," Österreichische Zeitschrift für Vermessung und Geoinformation (VGI), 91, 4; 223 – 235 (2003)
- [3] Blair, J., Rabine, D. and Hofton, M., "The Laser Vegetation Imaging Sensor: a medium-altitude, digitisation-only, airborne laser altimeter for mapping vegetation and topography," ISPRS Journal of Photogrammetry and Remote Sensing, 54, 115-122 (1999)
- [4] Harding, DJ, Carabajal, CC, "ICESat waveform measurements of within-footprint topographic relief and vegetation vertical structure," Geophysical Research Letters, Vol. 32, L21S10 (2005)
- [5] Wagner, W., Ullrich, A., Melzer, T., Briese, C., Kraus, K., "From singlepulse to full-waveform airborne laser scanners: Potential and practical challenges," International Archives of Photogrammetry, Remote Sensing and Spatial Information Sciences, XXXV-B3, 201-206 (2004)
- [6] Mallet, C., Bretar, F. "Full-waveform topographic lidar: State-of-the-art," ISPRS Journal of Photogrammetry and Remote Sensing, 64, 1-16 (2009)
- [7] Jalobeanu, A and Goncalves, G, "Robust Ground Peak Extraction With Range Error Estimation Using Full-Waveform LiDAR," IEEE Geoscience & Remote Sensing Letters, 11(7) (2014)
- [8] Yao, W., Krzystek, P., Heurich, M., "Identifying standing dead trees in forest areas based on 3D single tree detection from full waveform lidar data," ISPRS Annals, Volume I-7 (2012)
- [9] Wagner, W., Ullrich, A., Ducic, V., Melzer, T., Studnicka, N., "Gaussian decomposition and calibration of a novel small-footprint full-waveform digitising airborne laser scanner," ISPRS Journal of Photogrammetry & Remote Sensing, 60(2), 100-112 (2006)
- [10] Fieber, K.D., Davenport, I.J., Ferryman, J.M., Gurney, R.J., Walker, J.P., Hacker, J.M., "Analysis of full-waveform LiDAR data for classification of an orange orchard scene," ISPRS Journal of Photogrammetry and Remote Sensing, 82, 63–82 (2013)
- [11] Shendryk, I., Broich, M., Tulbure, M.G., Alexandrov, S.V., "Bottom-up delineation of individual trees from full-waveform airborne laser scans in a structurally complex eucalypt forest," Remote Sensing of Environment, 173, 69–83, <http://dx.doi.org/10.1016/j.rse.2015.11.008>, (2016)
- [12] Xu, L., Li, D., Li, X., "A high success rate full-waveform lidar echo decomposition method," Meas. Sci. Technol., 27 (2016)
- [13] Neuenschwander, A.L.; Magruder, L.A.; Tyler, M., "Landcover classification of small-footprint, full-waveform lidar data," Journal Of Applied Remote Sensing, 3(1) (2009)
- [14] Leigh, H.W.; Magruder, L.A.; "Using dual-wavelength, full-waveform airborne lidar for surface classification and vegetation characterization", Journal Of Applied Remote Sensing, 10(4), (2016)
- [15] Hancock, S., Anderson, K, Disney, M., Gaston, K.J., "Measurement of fine-spatial-resolution 3D vegetation structure with airborne waveform lidar: Calibration and validation with voxelised terrestrial lidar," Remote Sensing of Environment 188, 37–50 (2017)
- [16] Isenburg, M, "Pulsewaves", <https://rapidlasso.com/pulsewaves> (4 April 2017)
- [17] Anonymous, "Harris Geospatial Products and Solutions", <http://www.harrisgeospatial.com/ProductsandSolutions.aspx> (4 April 2017)
- [18] Tyo, J.S., Konsolakis, A., Diersen, D.I., Olsen, R. C.; "Principal-components-based display strategy for spectral imagery"; IEEE Transactions on Geoscience and Remote Sensing 41(3), 708-718 (2003)